Hindawi
Shock and Vibration
Volume 2021, Article ID 1218956, 16 pages
https://doi.org/10.1155/2021/1218956

*Research Article*

# Optimal Allocation and Control of Magnetorheological Dampers for Enhancing Seismic Performance of the Adjacent Structures Using Whale Optimization Algorithm

**Xiufang Lin** [1,2] **and Weiqing Lin** [3]

[1]*College of Physics and Electronic Information Engineering, Minjiang University, Fuzhou 350108, China*
[2]*Key Laboratory of Advanced Motion Control, Fujian Province University, Fuzhou 350108, China*
[3]*College of Information and Mechatronics Engineering, Ningde Normal University, Ningde 352100, China*

Correspondence should be addressed to Weiqing Lin; linweiqing2024@163.com

Received 21 August 2021; Accepted 10 December 2021; Published 23 December 2021

Academic Editor: Rozaimi Ghazali



The control strategy for protecting adjacent structures from earthquake excitations is gaining increasing significance. In this study, to improve the seismic performance, a semiactive control strategy using magnetorheological (MR) dampers to couple the adjacent structures is proposed. In this control strategy, to fully exploit the performance of MR dampers, the allocation (including the locations and the number) and fuzzy logic controller (FLC) system of MR dampers are simultaneously optimally designed by whale optimization algorithm (WOA) with a special encoding scheme. Simulation results verify that WOA provides competitive performance compared with the other three metaheuristic algorithms in terms of solution quality and robustness. Compared with other semiactive control methods including on-off, linear quadratic regulator-clipped voltage law, and WOA-FLC (optimal allocation is not considered) methods, by using much less MR dampers, the proposed control strategy can exhibit more excellent overall performance in terms of reducing the seismic responses and mitigating pounding.

## 1. Introduction

The mutual collision between two adjacent buildings during the past major earthquakes has caused significant damage. For instance, in the 1985 Mexico City earthquake, over 40% of structures impacted mutually, and more than 15% of the structures collapsed due to the pounding [1]. In the Loma Prieta earthquake, it was reported that there were over 200 pounding cases [2]. Even though building codes were greatly improved subsequently, a multitude of cases of pounding can be observed, such as in the 2011 Christchurch earthquake [3]. In downtown areas where buildings were often built very close to each other due to limited land, devastating damages observed from seismic pounding are particularly frequent [4].

To avoid mutual pounding under earthquake excitations, most researchers proposed linking adjacent structures with passive or active control devices. Hadi and Uz [5] proposed using the passive and active dampers with optimal parameters to achieve the seismic response mitigation of the adjacent buildings. Zou et al. [6] investigated the effectiveness of the active control of the adjacent structures considering the pile-soil-structure interaction effects connected with an ideal hydraulic servo system. However, passive devices are limited to a specific range of vibration modes and lack of adaptability and versatility, and active devices highly rely on large electric power so that they will be useless and even increase the vibration amplitude once the power supply is cut off.

Semiactive control devices are highly reliable and significantly adaptable that can overcome the above-mentioned disadvantages of the passive control devices and active control devices. Therefore, recently more and more researchers have attempted to employ this kind of control

device to link the adjacent structures [7]. Magnetorheological (MR) dampers, as one kind of intelligent semiactive control device, are fail-safe when the control system breaks down and can offer high adaptability and large force capacity. They have become one of the most promising control devices to reduce the vibration responses in the field of engineering [8–10]. Katebi and Zadeh [11] and Lin et al. [12] employed MR dampers to interconnect the adjacent structures with different kinds of control algorithms. The results validated that MR dampers not only can suppress the structural vibration but also can prevent structures from colliding with each other to a certain extent. Al-Fahdawi et al. [7] investigated the control effects of connecting the adjacent buildings with MR dampers and hydraulic actuators. The results verified that compared with hydraulic actuators, MR dampers can achieve better control results for the structural responses.

Nowadays various control algorithms implemented for the MR dampers have been proposed, for example, Lyapunov method [13] and clipped optimal control [14], sliding mode control [15], $H_\infty$ control [16], neural network control [17], and fuzzy logic control (FLC) [18]. Among these control algorithms, the FLC method has been known as a popular method. It can easily handle uncertainties and high nonlinearities of the MR damper and can provide inherent stability to the closed-loop system. Besides, it can directly calculate the MR damper control signal from the structural responses without the requirement of calculating the system control force. Abdeddaim et al. [19] investigated the performance of the FLC method for the MR dampers, which connected two adjacent structures. The results showed that this control algorithm outperforms passive-on control, passive-off control, and on-off control methods, especially in the control of the displacement and acceleration responses.

However, the parameters of the fuzzy control system that must be correctly pre-etermined for the system to function properly are difficult to be selected, as they highly depend on expert experience. Especially, designing a multi-input-multi-output FLC system is much more sophisticated when multiple MR dampers are required to be installed. Recently, it has been verified that optimally designing the FLC with metaheuristic algorithms (MAs) is surprisingly effective and efficient. Mahmoodabadi et al. [20] adopted a particle swarm optimization (PSO) algorithm to optimize the FLC for nonlinear systems. The simulation results demonstrated the superiority of the PSO-based FLC strategy over other MAs. Lin et al. [12] proposed a modified crow search algorithm (CSA) to optimize the FLC parameters for the MR dampers with the consideration of soil-structure interaction. The results validated the effectiveness of this optimal FLC.

On the other hand, the optimal arrangement of MR dampers is vitally important to the control effect, especially for the high-rise structures. Ok et al. [21] pointed out that there is no necessity to connect the adjacent structures at every single floor and significant displacement response reduction is possible with less MR dampers. However, this literature did not provide a solution for the optimal arrangement of MR dampers. Uz and Hadi [22] provided the optimal distribution of MR dampers and fuzzy rules of FLC to control the adjacent buildings by the use of GA, but the mutation operation that is a typical operation of GA cannot be conducted due to the specified encoding strategy. Besides, there was only one output of the FLC, which meant that the optimal command voltages of all the MR dampers were the same.

Recently, a nature-inspired algorithm, called whale optimization algorithm (WOA), which mimics the hunting behavior of humpback whales in nature, is proposed to solve mathematical and engineering optimization problems [23]. The results showed that the WOA outperformed other several MAs. This algorithm exhibited high local optima avoidance and fast convergence speed and was very easy to be performed as it has only two main parameters to be adapted. It has gained more and more attention in the engineering field. Pham et al. [24] used WOA to optimize resource allocation in wireless and communication networks. The results demonstrated that among several state-of-the-art algorithms, WOA was very competitive. Ebrahimgol et al. [25] proposed the application of WOA in the exergy optimization of a nuclear power plant. The results proved that the overall thermal efficiency of the Bushehr nuclear power plant was increased from 33.66% to 36.42% by using WOA, and this algorithm outperformed GA and PSO in terms of local optima avoidance and convergence. In addition, WOA has also been successfully used to solve other challenging problems such as association rule mining using fuzzy logic system [26], underwater image matching [27], structural damage identification [28], and code smell detection [29].

In this study, an intelligent semiactive control strategy employing MR dampers as the connection devices of the adjacent structures is proposed to improve the seismic performance. In this control strategy, to better control the MR dampers, an encoding scheme for the WOA is proposed to simultaneously optimize the allocations and FLC system of the MR dampers, even when the controlled buildings are high-rise type and the FLC is a multi-input-multi-output system. To the best of our knowledge, the optimal design of the MR damper distribution and the control system are rarely simultaneously considered for the coupled adjacent structures. Besides, there have been no published literatures about solving this problem using the WOA technique.

The rest of the paper is organized as follows. Section 2 builds the mathematical model for the MR damper-based adjacent buildings and derives the corresponding motion equation. Section 3 provides an overview of the WOA. In Section 4, the encoding design and the optimization steps for the proposed semiactive control scheme are described. Section 5 examined the effectiveness of the proposed control method in comparison with different semiactive control methods through numerical tests by MATLAB. Finally, the conclusions are stated in Section 6.

## 2. Modelling the Coupled Adjacent Buildings

*2.1. Motion Equation of the System.* As shown in Figure 1, the adjacent buildings are idealized as linear shear types, the inline floors of which are rigidly connected with MR

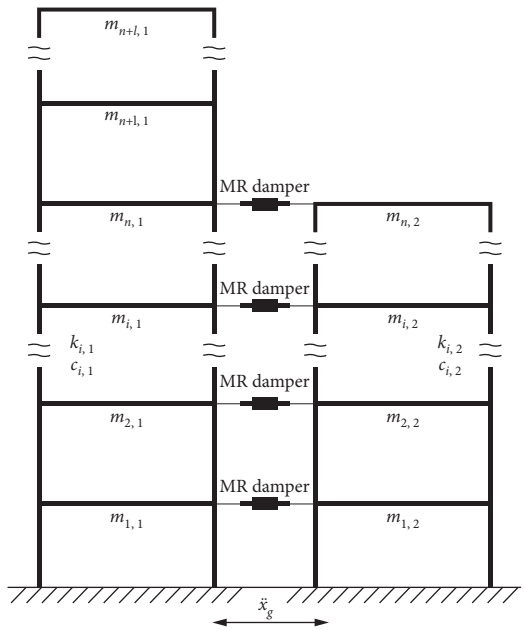


FIGURE 1: Schematic diagram of the MR dampers-coupled adjacent buildings.

dampers. Building 1 (the right building) and Building 2 (the left building) have $(n+l)$ stories and $n$ stories, respectively. Therefore, the coupled system has $(2n+l)$ degrees of freedom. In this figure, $\ddot{X}_{\mathbf{g}}(t)$ is the earthquake acceleration. Second subscripts 1 and 2 of every parameter refer to Buildings 1 and 2, respectively. For example, $m_{i,2}$, $k_{i,2}$, and $c_{i,2}$ denote the mass, stiffness, and damping, respectively, of the $i$-th floor of Building 2. The governing motion equation for the MR damper-coupled adjacent buildings can be expressed as follows:

$$\mathrm{M}\ddot{X}(t) + \mathrm{C}\dot{X}(t) + \mathrm{K}\mathrm{X}(t) = \Lambda\ddot{X}_g(t) + \Gamma\mathrm{F}(t), \tag{1}$$

where $\mathbf{F}(t) = \{f_1(t), f_2(t), \ldots, f_n(t)\}^{\mathrm{T}}$ represents damping forces of the MR dampers, $\mathbf{\Gamma}_{(2n+l,n)} = [\mathbf{\Gamma}_1, \mathbf{\Gamma}_2, \ldots, \mathbf{\Gamma}_n]$ is the distribution matrix of the damping forces, $\mathbf{\Lambda}$ is a distribution vector of the seismic excitation, $\mathbf{X}(t)$ is the relative displacement to the ground (called displacement in short), and $\dot{\mathrm{X}}(t)$ and $X(t)$ are the velocity and acceleration vectors of the system, respectively. $\mathbf{X}(t)$ is expressed as follows:

$$\mathrm{X}(t) = \left\{ \begin{array}{l} x_{1,1}(t), x_{2,1}(t), x_{i,1}(t), \ldots, x_{n+l,1}(t) \\ x_{1,2}(t), x_{2,2}(t), x_{i,2}(t), \ldots, x_{n,2}(t) \end{array} \right\}^T_{(2n+l,1)}, \tag{2}$$

where $x_{i,1}$ and $x_{i,2}$ are the relative displacements of the $i$-th floors of Buildings 1 and 2, respectively.

In equation (1), **M**, **C**, and **K** are mass, damping, and stiffness matrices of the coupled system, respectively, which are expressed as follows:

$$\begin{aligned} \mathrm{M} &= \begin{bmatrix} \mathrm{M}_1 & \\ & \mathrm{M}_2 \end{bmatrix}_{(2n+l,2n+l)}, \\ \mathrm{K} &= \begin{bmatrix} \mathrm{K}_1 & \\ & \mathrm{K}_2 \end{bmatrix}_{(2n+l,2n+l)}, \\ \mathrm{C} &= \begin{bmatrix} \mathrm{C}_1 & \\ & \mathrm{C}_2 \end{bmatrix}_{(2n+l,2n+l)}. \end{aligned} \tag{3}$$

$\mathbf{M_1}$, $\mathbf{C_1}$, and $\mathbf{K_1}$ are mass, damping, and stiffness matrices of Building 1, respectively, which are calculated by the following equations. The corresponding matrices $\mathbf{M_2}$, $\mathbf{C_2}$, and $\mathbf{K_2}$ of Building 2 can be calculated similarly.

$$\begin{aligned} \mathrm{M}_1 &= \begin{bmatrix} m_{1,1} & & & \\ & m_{2,1} & & \\ & & \ddots & \\ & & & m_{n+l,1} \end{bmatrix}_{(n+l,n+l)}, \\ \mathrm{K}_1 &= \begin{bmatrix} k_{1,1}+k_{2,1} & -k_{2,1} & & \\ -k_{2,1} & \ddots & & \\ & & k_{(n+l-1),1}+k_{n+l,1} & -k_{n+l,1} \\ & & -k_{n+l,1} & k_{n+l,1} \end{bmatrix}_{(n+l,n+l)}, \\ \mathrm{C}_1 &= \begin{bmatrix} c_{1,1}+c_{2,1} & -c_{2,1} & & \\ -c_{2,1} & \ddots & & \\ & & c_{(n+l-1),1}+c_{n+l,1} & -c_{n+l,1} \\ & & -c_{n+l,1} & c_{n+l,1} \end{bmatrix}_{(n+l,n+l)}. \end{aligned} \tag{4}$$

If $\mathrm{Z}(t) = [\mathrm{X}(t), \dot{\mathrm{X}}(t)]^T_{(2\times(2n+l),1)}$ represents state variable; then we can rewrite equation (1) as follows:

$$\dot{\mathrm{Z}}(t) = \mathrm{A}\mathrm{Z}(t) + \mathrm{B}_g\ddot{\mathrm{X}}_g(t) + \mathrm{B}_f\mathrm{F}(t). \tag{5}$$

**A** is the system matrix; $\mathbf{B_g}$ and $\mathbf{B_f}$ are the distribution matrices of the seismic excitation and the damping forces, respectively. These three matrices are defined as follows:

$$\begin{aligned} \mathrm{A} &= \begin{bmatrix} 0 & \mathrm{I} \\ -\mathrm{M}^{-1}\mathrm{K} & -\mathrm{M}^{-1}\mathrm{C} \end{bmatrix}_{(2\times(2n+l),2\times(2n+l))}, \\ \mathrm{B}_g &= \begin{bmatrix} 0 \\ -\Lambda \end{bmatrix}_{(2\times(2n+l),1)}, \\ \mathrm{B}_f &= \begin{bmatrix} 0 \\ \mathrm{M}^{-1}\Gamma \end{bmatrix}_{(2\times(2n+l),n)}, \end{aligned} \tag{6}$$

where **I** denotes the unit matrix and **0** represents the zero matrix (vector).

If $\ddot{\mathrm{X}}_a(t)$ denotes the absolute acceleration (called the acceleration in short in the following sections) of the coupled system, then the output of the system $\mathrm{Y}(t) = [\mathrm{X}(t)^T, \dot{\mathrm{X}}(t)^T, \ddot{\mathrm{X}}_a(t)^T]^T$ can be re-expressed by

$$\mathrm{Y}(t) = \mathrm{C}_z \mathrm{Z}(t) + \mathrm{D}_f \mathrm{F}(t), \tag{7}$$

where

$$\mathrm{C}_z = \begin{bmatrix} \mathrm{I} & 0 \\ 0 & \mathrm{I} \\ -\mathrm{M}^{-1}\mathrm{K} & -\mathrm{M}^{-1}\mathrm{C} \end{bmatrix}_{(3\times(2n+l),2\times(2n+l))}, \quad \mathrm{D}_f = \begin{bmatrix} 0 \\ 0 \\ \mathrm{M}^{-1}\Gamma \end{bmatrix}_{(3\times(2n+l),n)}. \tag{8}$$

In order to conveniently conduct the simulation calculation, we describe equations (5) and (7) in the form of standard state-space as follows:

$$\begin{cases} \dot{\mathrm{Z}}(t) = \mathrm{A}\mathrm{Z}(t) + \mathrm{B}\mathrm{U}(t), \\ \mathrm{Y}(t) = \mathrm{C}_z \mathrm{Z}(t) + \mathrm{D}_f \mathrm{U}(t), \end{cases} \tag{9}$$

where $\mathbf{Y}(t)$ is the output vector of the system; $\mathbf{B}$, $\mathbf{C_z}$, and $\mathbf{D_f}$ are the statement matrices; and $\mathbf{U}(t)$ is the input vector. $\mathbf{B}$ and $\mathbf{U}(t)$ are expressed as follows:

$$\mathrm{B} = \begin{bmatrix} \mathrm{B}_g \\ \mathrm{B}_f \end{bmatrix}_{(2\times(2n+l),(1+n))}, \quad \mathrm{U}(t) = \begin{bmatrix} \ddot{\mathrm{X}}_g(t) \\ \mathrm{F}(t) \end{bmatrix}_{((1+n),1)}, \tag{10}$$

where $\ddot{\mathrm{X}}_a(t)$ is the absolute acceleration (called acceleration in short in the following section) of the coupled system.

*2.2. Damping Force of the MR Damper.* The phenomenological model is widely used to portray the dynamic behaviors of the MR damper that can accurately relate to the voltage-dependent parameters and damping force [30]. As for the above-mentioned adjacent building system, by using this model, the equation governing the damping force is expressed as follows:

$$F = c_1 \dot{y}_i + k_1\left(x_{i,1} - x_{i,2} - x_0\right), \tag{11}$$

where $x_{i,1}$ and $x_{i,2}$ are the displacements of the $i$-th floor of Buildings 1 and 2, respectively. $k_1$ presents the accumulator stiffness. $x_0$ is the initial displacement for the spring element. $c_1$ is viscous damping at a low velocity.

$$\dot{y}_i = \frac{1}{(c_0 + c_1)}\left\{\alpha z_i + c_0\left(\dot{x}_{i,1} - \dot{x}_{i,2}\right) + k_0\left(\dot{x}_{i,1} - \dot{x}_{i,2} - y_i\right)\right\}, \tag{12}$$

where $\dot{x}_{i,1}$ and $\dot{x}_{i,2}$ are the velocities of the $i$-th floor of Buildings 1 and 2, respectively. $c_0$ is viscous damping at the high velocity; $\alpha$ denotes a factor related to the hysteresis loop; $k_0$ represents the stiffness constant at the high velocity. $c_1$, $\alpha$, and $c_0$ in equations (11) and (12) are estimated as functions of the input voltage of the MR damper [30]. The evolutionary variable $z_i$ is given by

$$\dot{z}_i = -\gamma\left|\dot{x}_{i,1} - \dot{x}_{i,2} - \dot{y}\right|z_i\left|z_i\right|^{n-1} - \beta\left(\dot{x}_{i,1} - \dot{x}_{i,2} - \dot{y}_i\right)\left|z_i\right|^n + A\left(\dot{x}_{i,1} - \dot{x}_{i,2} - \dot{y}_i\right), \tag{13}$$

where $\gamma$, $\beta$, and $A$ are shape parameters of the hysteresis loop.

## 3. Overview of WOA

In the whale optimization algorithm (WOA), the position of prey corresponds to the global optimal solution of the problem. The algorithm initializes with random positions. These positions are updated by search agents to become randomly selected positions or the best positions in each iteration. The algorithm is acquired by the mathematical model that conducts the following encircling prey and bubble net feeding for the search agents to update their positions. The flowchart of the WOA is shown in Figure 2.

Firstly, the humpback whales can identify the position of the prey and encircle them. Since the optimum solution is unknown at the beginning, the optimal position in the current population is assumed to be the prey location or is close to the optimum. After the best search agent is specified, other search agents will try to update their positions to move toward the best search agent. This behavior is achieved by using the following equation:

$$X(t+1) = X^* - A \cdot \left|C \cdot X^*(t) - X(t)\right|, \tag{14}$$

where $t$ is the iteration, $X$ is the position vector, and $X^*$ is the best position obtained so far. $A$ and $C$ are coefficient vectors that are expressed as follows:

$$A = 2a \cdot r - a, \tag{15}$$

$$C = 2 \cdot r, \tag{16}$$

where $a$ is linearly decreased from 2 to 0 over the course of iterations and $r$ is a random vector where random numbers are uniformly distributed in the interval [0, 1]. The value ranges set for $a$ and $r$ can make the search vector $A$ be adaptive variation, which can allow the WOA to smoothly transit between exploration and exploitation [23].

Then, the bubble net hunting with two methods including shrinking encircling and spiral updating position is conducted. The shrinking encircling mechanism is realized by decreasing the control parameter $a$ in equation (15). Accordingly, the value of $A$ is in the range of $[-a, a]$ due to equation (15). The following mathematical model is used to describe the spiral updating position operation.

$$X(t+1) = D'' \cdot e^{bl} \cdot \cos(2\pi l) + X^*(t), \tag{17}$$

where $D'' = |X^*(t) - X(t)|$ indicates the distance of the $i$-th whale to the best prey found so far. $b$ is a constant to define the shape of the logarithmic spiral. $l$ is a random number in $[-1, 1]$. It should be noted that whales swim in a combination path, that is, the contraction circle of their prey and a spiral path. In order to simulate this behavior, the probability of 50% is considered as follows:

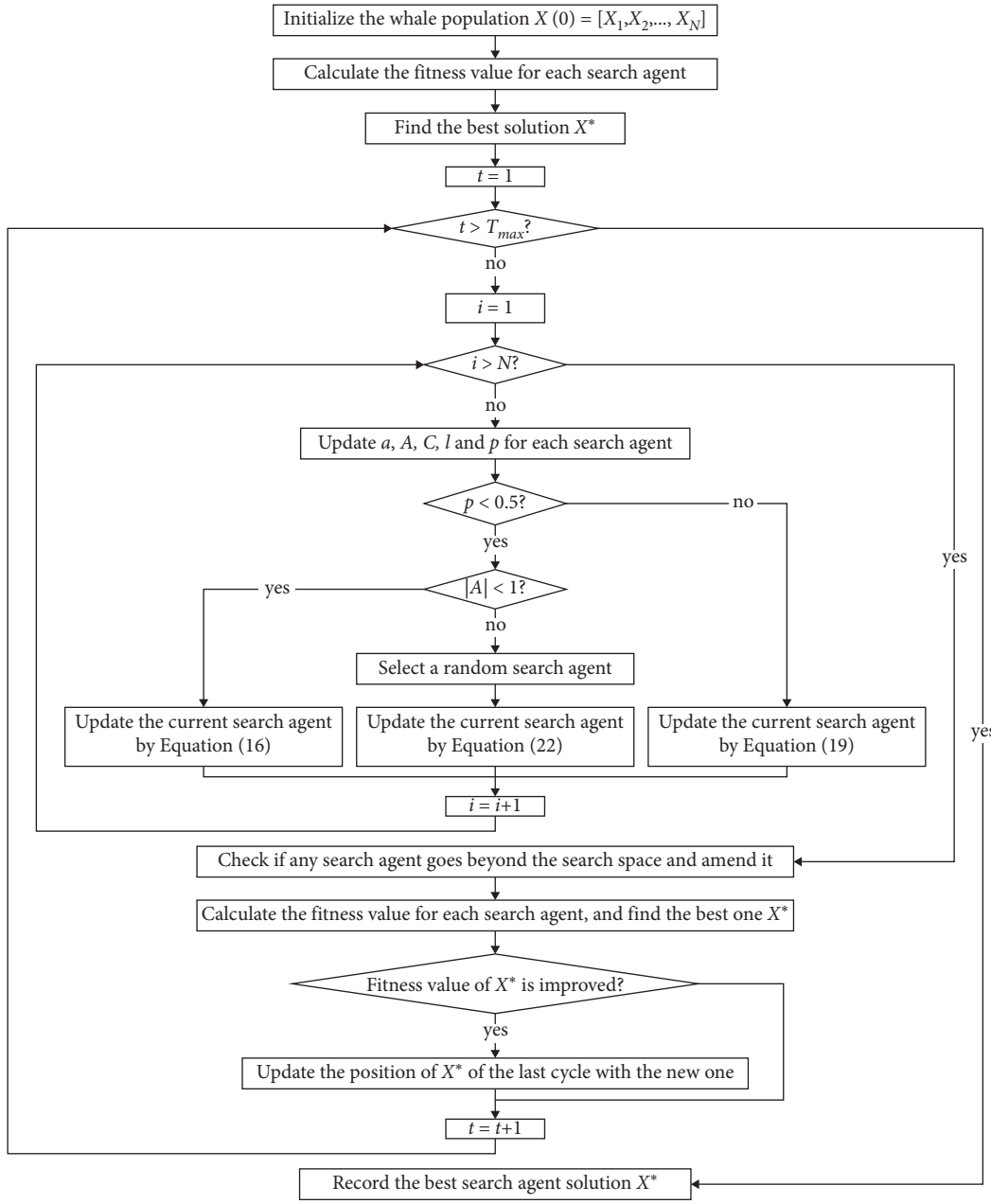


Figure 2: Flowchart of WOA.

$$X(t+1) = X^*(t) - A \cdot \left|C \cdot X^*(t) - X(t)\right| \quad \text{if } p < 0 \cdot 5,$$
$$X(t+1) = D'' \cdot e^{bl} \cdot \cos(2\pi l) + X^*(t) \quad \text{if } p \geq 0 \cdot 5, \tag{18}$$

where $p$ is a random number in [0, 1]. Based on this value, the algorithm is able to switch between either a spiral or circular movement.

Besides bubble-net predation, whales can also search for food randomly. The whale individuals search at random according to each other's position, and this model can be expressed as follows:

$$X(t+1) = X_{\text{rand}} - A \cdot \left|C \cdot X_{\text{rand}}(t) - X(t)\right|, \tag{19}$$

where $X_{\text{rand}}$ is a random position vector chosen from the current population.

## 4. The Proposed WOA-ALLO-FLC Method

To design the allocation of the MR dampers and the FLC with satisfactory performance with the WOA, the key step is to design a proper encoding structure for each whale individual in relation to the parameters to be determined, which will be detailed in the next subsection.

*4.1. Design of the Encoding Strategy.* To begin with, the FLC parameters and the encoding strategy for fuzzy rules are described as follows:

The controller is designed with $n_{\mathrm{i}}$ inputs and $n_{\mathrm{o}}$ outputs using $n_{\mathrm{imf}}$ MFs for each input and $n_{\mathrm{omf}}$ MFs for each output. Accordingly, $n_{\mathrm{imf}}$ linguistic values are used to denote the MFs for each input variable, for example, negative, zero, and positive. Similarly, the MFs for each output variable are denoted by $n_{\mathrm{omf}}$ linguistic values, for example, large, medium, and zero. The input universes of discourse (UOD) and output UOD are normalized over [−1, 1] and [0, 2], respectively. Assume the maximum voltage is $V_{\max}$, then let all the output scaling factors be equal to $V_{\max}/2$. Reciprocals of the input scaling gains are set to be 50% of the corresponding input accelerations.

The fuzzy rules should be designed appropriately that is to describe the relationship between inputs and outputs of the controller by using the "if-then" form. For example, rule $i$: if $x_1$ is $A_1^i$, $x_2$ is $A_{2,}^i \ldots$, and $x_{Nin}$ is $A_{n_i}^i$, then $y$ is $B_i$, where $x_1$, $x_2, \ldots, x_{n_i}$ are the input variables of the FLC; $y$ is the output variable; $A_1^i$, $A_2^i, \ldots, A_{n_i}^i$ are the linguistic values of input variables; $B_i$ is the fuzzy subset of the output variable. If the antecedent parameters of the rules use all the possible combinations of all the inputs, the number of the fuzzy rules is

$$n_{\mathrm{rule}} = n_o \times \left(n_{imf}\right)^{n_i}. \tag{20}$$

After the structure of the FLC system is determined, the input for each rule will be accordingly determined. Therefore, in the fuzzy rules, only the output linguistic variables require encoding. In this study, the $n_{\mathrm{imf}}$ input linguistic variables are encoded with continuous integers from 1 to $n_{\mathrm{imf}}$. For example, a string of codes that represents the fuzzy rule can be expressed as follows:

$$\left[\overbrace{1\ 1\ 5\ 3\ 1\ n_{imf}\ 4\ 1\ 2n_{imf}\ 4\ \ldots\ 5}^{n_{\mathrm{rule}}}\right]. \tag{21}$$

Next, the design of the encoding strategy for the distribution of MR dampers is proposed as follows:

For the sake of simplicity, let the different MR dampers linking the same adjacent floors generate the same damping force. According to equations (1) and (8), the optimization process is actually the process of determining the distribution matrix of the damping forces $\mathbf{\Gamma}_{(2n+l,n)} = [\mathbf{\Gamma}_1, \mathbf{\Gamma}_2, \ldots, \mathbf{\Gamma}_n]$. Based on the analysis of the motion equation in Section 2, it can be deduced that the $i$-th column vector of $\mathbf{\Gamma}_{(2n+l,n)}$ as shown below means that the $i$-th adjacent floors are not be connected with any MR dampers:

$$\Gamma(:, i) = \Gamma_i = \left[\overbrace{0\ 0\ \cdots\ 0\ 0\ \cdots\ 0}^{n+l}\ \ \overbrace{0\ 0\ \cdots\ 0\ 0\ \cdots\ 0}^{n}\right]^T. \tag{22}$$

Besides, the $j$-th column vector of $\mathbf{\Gamma}_{(2n+l,n)}$ as shown below means that the $j$-th adjacent floors are connected with one MR damper:

$$\Gamma(:, j) = \Gamma_j = \left[\overbrace{0\ 0\ \cdots\ -1\ 0\ 0\cdots\ 0}^{n+l}\ \ \overbrace{0\ 0\ \cdots\ 1\ 0\ 0\cdots\ 0}^{n}\right]^T, \tag{23}$$

where −1 is in the $j$-th row and 1 is in the $(j+n+l)$-th row. Therefore, it can be concluded that if there are 5 pairs of adjacent floors are connected, including the 2nd, 4th, 6th, 8th, and 10th floors, then $\mathbf{\Gamma}_{(2n+l,n)}$ can be expressed as follows:

$$\Gamma_{(2n+l,n)} = \left[\begin{array}{cc}
\overbrace{\begin{array}{cccccccccccccc}
0 & & & & & \cdots & & & & & & & & 0 \\
0 & -1 & 0 & & & \cdots & & & & & & & & 0 \\
0 & & & & & \cdots & & & & & & & & 0 \\
0 & 0 & 0 & -1 & 0 & & & \cdots & & & & & & 0 \\
0 & & & & & \cdots & & & & & & & & 0 \\
0 & 0 & 0 & 0 & 0 & -1 & 0 & & \cdots & & & & & 0 \\
0 & & & & & \cdots & & & & & & & & 0 \\
0 & 0 & 0 & 0 & 0 & 0 & 0 & -1 & 0 & \cdots & & & & 0 \\
0 & & & & & \cdots & & & & & & & & 0 \\
0 & 0 & 0 & 0 & 0 & 0 & 0 & 0 & 0 & -1 & 0 & \cdots & & 0 \\
0 & & & & & \cdots & & & & & & & & 0 \\
\vdots & & & & & & & & & & & & & \vdots \\
0 & & & & & \cdots & & & & & & & & 0
\end{array}}^{n+l} &
\overbrace{\begin{array}{cccccccccccccc}
0 & & & & & \cdots & & & & & & & & 0 \\
0 & 1 & 0 & & & \cdots & & & & & & & & 0 \\
0 & & & & & \cdots & & & & & & & & 0 \\
0 & 0 & 0 & 1 & 0 & & & \cdots & & & & & & 0 \\
0 & & & & & \cdots & & & & & & & & 0 \\
0 & 0 & 0 & 0 & 0 & 1 & 0 & & \cdots & & & & & 0 \\
0 & & & & & \cdots & & & & & & & & 0 \\
0 & 0 & 0 & 0 & 0 & 0 & 0 & 1 & 0 & \cdots & & & & 0 \\
0 & & & & & \cdots & & & & & & & & 0 \\
0 & 0 & 0 & 0 & 0 & 0 & 0 & 0 & 0 & 1 & 0 & \cdots & & 0 \\
0 & & & & & \cdots & & & & & & & & 0 \\
\vdots & & & & & & & & & & & & & \vdots \\
0 & & & & & \cdots & & & & & & & & 0
\end{array}}^{n}
\end{array}\right]^T. \tag{24}$$

Based on the above analysis, once the first $n$ rows are determined, the last $n$ rows will be determined accordingly because the position relationship of –1 and 1 are fixed in the nonzero column vectors. Therefore, the problem that which adjacent floors are connected with MR dampers can be solved by determining the positions of –1 in the first $n$ rows of $\mathbf{\Gamma}_{(2n+l,n)}$.

Finally, the encoding strategy for the allocations of MR dampers is designed as follows: the length of the string of codes is $n$. Real-value coding is employed. Coding numbers are continuous integers ranging from 0 to $n_{\text{maxD}}$, where $n_{\text{maxD}}$ is the allowed maximum number of MR dampers linking the adjacent floors of the same height. The total number of nonzero codes is equal to the total number of the pairs of the connected adjacent floors, and the number $k$ in the $i$-th place represents that the $i$-th adjacent floors are connected by $k$ MR dampers. For example, a string of codes listed as below means that the 2nd, 4th, 6th, 8th, and 10th adjacent floors are connected by 1, 3, $n_{\text{maxD}}$, 1, and $n_{\text{maxD}}$ MR dampers, respectively.

$$\left[\overbrace{0\ 1\ 0\ 3\ 0\ n_{\max D}\ 0\ 1\ 0 n_{\max D}\ 0\ \cdots\ 0}^{n}\right]. \tag{25}$$

This string of codes contains the information of the location and number of the MR dampers, and it corresponds to $\mathbf{\Gamma}_{(2n+l,n)}$ in equation (29) in terms of the location of the MR dampers.

In conclusion, in this study, the total number of the parameters to be optimized is equal to $(n_{\text{rule}} + n)$.

*4.2. Design Process of the Control Strategy.* The specific steps of the design process for the proposed control method are detailed as follows:

*Step 1.* Determine the main parameters of the FLC including the MF type, number of MFs for each input/output $n_{\text{imf}}$ and $n_{\text{omf}}$, and number of inputs/outputs $n_{\text{i}}$ and $n_{\text{o}}$. Then calculate the number of the fuzzy rules $n_{\text{rule}}$.

*Step 2.* According to the coupled structural parameters, determine the number of the state-space equation matrices including $\mathbf{A}$, $\mathbf{B_g}$, and $\mathbf{C_z}$ defined in equations (6) and (8). Calculate the uncontrolled structural responses and determine the input scaling gains of the FLC. Determine the output scaling gains of the FLC based on the maximum voltage value of the chosen MR damper.

*Step 3.* Determine the total number of parameters to be optimized denoted as $N_{\text{para}}$. Define the fitness function and let it be equal to the objective function (see equation (26)).

*Step 4.* Specify the maximum total number of MR dampers employed $N_{\text{maxD}}$ and provide the parameter boundaries for the damper allocation and the fuzzy rules according to the $n_{\text{maxD}}$ defined in Section 4.1 and $n_{\text{imf}}$, respectively.

*Step 5.* Initialize the WOA parameters, such as the population size $N$ and iteration number $T_{\max}$. Randomly generate initial position $X(0) = [X_1,\ X_2,\ \cdots,\ X_N]$ for the population, and let the initial best fitness value be equal to 1 as this is a minimization problem.

*Step 6.* $t = 0$. Start the iteration process.

*Step 7.* is shown in Table 1.

*Step 8.* For the whole population, update the best position $X^*$.

*Step 9.* is shown in Table 2.

*Step 10.* Judge whether $t \le T_{\max}$. If yes, repeat Steps 7–9; else go to Step 11.

*Step 11.* Find out the global best position $X^*$. Determine the optimal MR damper allocation and the optimal FLC system.

## 5. Numerical Study

The adjacent 20-storey building (Building 1) and 10-storey building (Building 2) are linked with MR dampers with a maximum force capacity of 1,000 kN [31]. The structural parameters including mass, stiffness, and damping coefficient for both buildings are listed in Table 3. Considering that the 1940 El Centro earthquake is a far-field historical ground motion record usually chosen as the seismic excitation for the optimization design of the semiactive control strategy with MR dampers [32–34], in this study, this earthquake is also selected as the excitation of the buildings.

*5.1. The Optimization Results and Algorithm Comparison.* The parameter conditions for the encoding strategy are listed in Table 4. The top floor accelerations of both buildings are set to be inputs. Assume that every pair of the adjacent floors are connected and controlled. Therefore, the FLC to be designed is a 2-input-10-output system. The linguistic values for each input variable include negative (N), zero (ZO), and positive (P), and the linguistic values for each output variable include large (L), medium (M), and zero (ZO). For each input and output, the membership functions using a generalized bell-shaped type are shown in Figure 3.

For the sake of the security of the structure and the occupants in the buildings, the maximum displacements of both buildings are required to be reduced. Therefore, we define the objective function as follows:

$$Obj = \alpha J_{1,1} + (1 - \alpha) J_{1,2}, \tag{26}$$

where $\alpha$ is a weighting coefficient.

$$J_{1,1}, J_{1,2} = \frac{\max\left|x^c(t)\right|}{\left|x^{unc}_{\max}\right|}. \tag{27}$$

The second subscripts of $J_{1,1}$ and $J_{1,2}$ refer to Buildings 1 and 2, respectively. $x^{unc}_{\max}$ is the maximum uncontrolled

Table 1: The pseudocode of Step 7 of the design process.

For each individual position, calculate the fitness value with the following steps:
**Judge** whether the total number of MR dampers is smaller than $N_{\text{maxD}}$.
**If yes**,
    find out the information of the MR damper allocation, including which pairs of adjacent floors are linked by MR dampers and corresponding damper number for each pair of the adjacent floor
    determine the matrices $\mathbf{\Gamma}_{(2n+l,n)}$, $\mathbf{B}$, and $\mathbf{D_f}$ defined in equations (1), (10), and (8), respectively
    generate an FLC
    calculate the fitness value according to the objective function
**else**
    let the fitness value = 1
**end**

Table 2: The pseudocode of Step 9 of the design process.

Update each position $X_i$ ($i \in [1, N]$) with the following steps:
Update the algorithm parameters including $a$, $b$, $A$, $C$, $l$, and $p$ defined in Section 3
**Judge** whether $p < 0.5$
**If yes,**
    **Judge** whether $|A| \geq 1$, which is defined in Section 3
    **If yes,**
        randomly determine a position $X_{rand}$ in the range of the current population, and update the position Xi according to equation (19)
    **else**
        update the position Xi based on $X^*$ according to equation (14)
    **end**
**else**
    conduct spiral position updating according to equation (17)
**end**
**Judge** whether every code of the position $X_i$ is within the predefined value ranges
**If yes**,
    keep the position $X_i$
**else**
    replace the code of the position $X_i$ with the corresponding limit value
**end**
$t = t + 1$

Table 3: Structural parameters of the adjacent buildings [31].

| Parameters | Structure 1 | Structure 2 |
|---|---|---|
| Number of stories | 20 | 10 |
| Structural mass, $m_i$ | $8 \times 10^5$ kg | $m_1 = 2.15 \times 10^5$ kg<br>$m_i = 2.01 \times 10^5$ kg, $i = 2, 3, \ldots, 7$<br>$m_i = 2.03 \times 10^5$ kg, $i = 8, 9$<br>$m_i = 1.76 \times 10^5$ kg, $i = 10$ |
| Structural stiffness, $k_i$ | $1.4 \times 10^9$ N/m | $k_1 = 4.68 \times 10^8$ N/m, $k_2 = 4.76 \times 10^8$ N/m<br>$k_3 = 4.68 \times 10^8$ N/m<br>$k_i = 4.5 \times 10^8$ N/m, $i = 4, 5, 6, 7$<br>$k_i = 4.37 \times 10^8$ N/m, $i = 8, 9$<br>$k_i = 3.12 \times 10^8$ N/m, $i = 10$ |
| Structural damping, $c_i$ | $4.375 \times 10^6$ Ns/m | $c_1 = 1.676 \times 10^6$ Ns/m, $c_2 = 1.648 \times 10^6$ Ns/m<br>$c_3 = 1.585 \times 10^6$ Ns/m, $c_4 = 1.585 \times 10^6$ Ns/m<br>$c_5 = 1.539 \times 10^6$ Ns/m, $c_6 = 1.539 \times 10^6$ Ns/m<br>$c_7 = 1.539 \times 10^6$ Ns/m, $c_8 = 1.539 \times 10^6$ Ns/m<br>$c_9 = 1.099 \times 10^6$ Ns/m, $c_{10} = 1.146 \times 10^6$ Ns/m |

displacement of each building. $x^c(t)$ is the controlled displacement of the corresponding floor of each building. In this study, to determine the value of the weighting coefficient $\alpha$ in equation (26), the analysis about the compromises between the objectives $J_1$ and $J_2$ is conducted, as shown in Figure 4.

Table 4: Parameter conditions for the encoding strategy.

| Parameter | Value | Parameter | Value |
|---|---|---|---|
| $n$ | 10 | $n_{\mathrm{i}}$ | 2 |
| $N_{\mathrm{maxD}}$ | 20 | $n_{\mathrm{imf}}/n_{\mathrm{omf}}$ | 3 |
| $n_{\mathrm{maxD}}$ | 4 | $n_{\mathrm{rule}}$ | 90 |
| $n_{\mathrm{o}}$ | 10 | $N_{\mathrm{para}}$ | 100 |

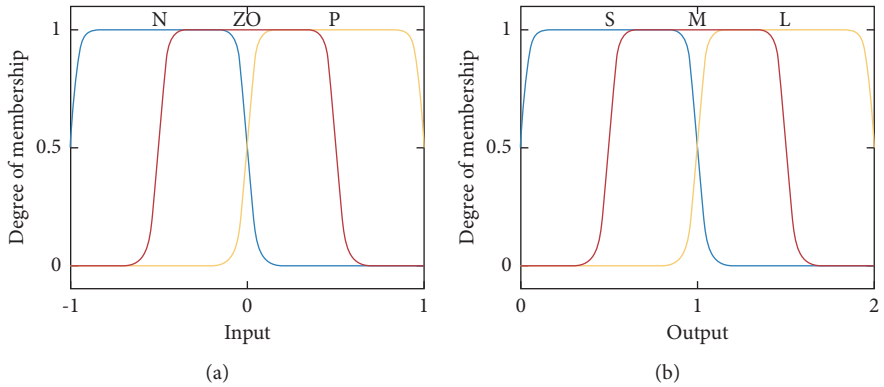


Figure 3: Membership functions (MFs): (a) input MFs and (b) output MFs.

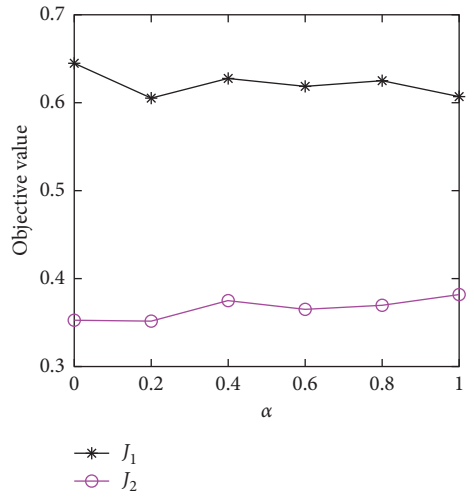


Figure 4: The variation of objective values $J_1$ and $J_2$ with different $\alpha$.

As seen from Figure 4, simultaneously minimizing both objectives cannot be realized in the optimization whatever $\alpha$ is. Nevertheless, this figure indicates that when $\alpha = 0.2$ an excellent comprehensive control effect in terms of both displacement responses can be obtained. Therefore, $\alpha = 0.2$ is adopted as the weight value of the objective function in the subsequent studies.

GA [21, 22, 32] and PSO [20] are metaheuristic algorithms that search the optimal solution via simulating natural evolutionary process and via simulating migration and clustering behavior of birds, respectively. These two algorithms are often used as benchmarks for algorithm comparison [25]. Therefore, in this study, GA, PSO, and CSA [35] are used for comparison to validate the performance of WOA. The controlling parameters of these three algorithms are listed in Table 5. Other parameters for all of these algorithms are chosen as: population size $N = 20$, iteration number $T_{\max} = 100$, independent runs = 30. The convergence curves of the best solutions for these algorithms are shown in Figure 5.

The figure shows that among these four algorithms, WOA can achieve the smallest objective value. Detail results for the objective values including the best, mean, worst, and standard deviation (Std. Dev.) values are listed in Table 6. The table demonstrates that among these four indices for the objective value, WOA can obtain three better quantities than its competitors. WOA performs best in terms of convergence accuracy as it can obtain the smallest mean value. The robustness of WOA is very competitive as it comes second to that of CSA in terms of the Std. Dev. value.

Table 5: Controlling parameters of the metaheuristic algorithms.

| Algorithm | Parameter | Value |
|---|---|---|
| GA | Crossover probability | 0.9 |
| | Mutation probability | 0.2 |
| PSO | Learning factor 1 | 1.5 |
| | Learning factor 2 | 1.5 |
| | Inertia weight | 0.73 |
| CSA | Flight length | 2 |
| | Awareness probability | 0.1 |

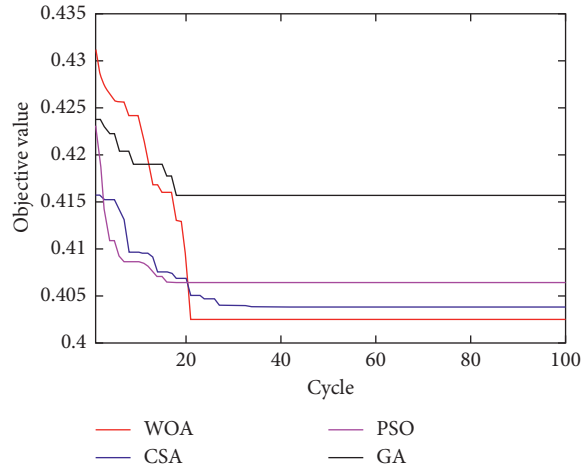


Figure 5: Convergence curves of the best solutions for different algorithms.

Table 6: Comparison of objective values among different methods.

| Objective values | GA | PSO | CSA | WOA |
|---|---|---|---|---|
| Best | 0.41564 | 0.40636 | 0.40378 | 0.40247 |
| Mean | 0.4212 | 0.41104 | 0.40752 | 0.40557 |
| Worst | 0.42386 | 0.41815 | 0.41084 | 0.40914 |
| Std. Dev. | 0.0022 | 0.00265 | 0.00197 | 0.00205 |

The optimal results obtained with the proposed WOA-ALLO-FLC are shown as follows: The allocation of the MR dampers is that all the 8th, 9th, and 10th adjacent floors are connected with 4 MR dampers. That means the total number of MR dampers is 12 although $N_{\max D}$ is set to be 20. The optimal fuzzy rules are listed in Table 7. Since only the top three adjacent floors are linked, as for the fuzzy rules, in the practical application what we concern about are only the linguistic values in bold font in the table. Accordingly, the curve surfaces of fuzzy rules for the top three floors are presented in Figure 6.

*5.2. Performance Comparison among Different Control Strategies.* The control results of the proposed WOA-ALLO-FLC method using only 12 MR dampers are compared with those of on-off control [12], linear quadratic regulator based on clipped voltage law (LQR-CVL) [12] where LQR is a linear quadratic optimal control with the full-state feedback as input that is often used for calculating the desired controlling force [6, 13, 14], and WOA-FLC methods where only the FLC is optimized with WOA using the proposed encoding scheme. In the latter three control methods, every pair of adjacent floors are connected with two MR dampers. That is, a total number of 20 MR dampers are employed in these three control methods.

The control results of the peak displacements of all the floors with different control methods for Buildings 1 and 2 are shown in Figures 7 and 8, respectively. As for Building 1, it is obvious that WOA-ALLO-FLC outperforms the other three control methods, and LQR-CVL performs better than WOA-FLC and on-off methods. As for Building 2, the control effect of the WOA-FLC control is close to that of WOA-ALLO-FLC. However, the maximum displacement is controlled slightly better by WOA-ALLO-FLC. Besides, the on-off control outperforms the LQR-CVL control. Table 8 lists the control results of the maximum displacements, where the reduction ratios of the responses with and without control are listed in the parentheses. Among all these control strategies, WOA-ALLO-FLC achieves the best control effects of the maximum displacements for Buildings 1 and 2 with the reduction ratio of 39% and 65%, respectively, which coincides with the objective of the optimization with WOA as shown in equation (26).

Table 7: Fuzzy inference rule base.

| Input 1 | Input 2 | | |
|---|---|---|---|
| | *N* | ZO | *P* |
| *N* | S/S/L/L/L/L/L/**L**/**M**/**L** | L/L/M/L/L/L/L/**L**/**S**/**M** | S/L/L/S/L/L/M/**S**/**S**/**L** |
| ZO | S/S/M/L/L/L/L/**S**/**L**/**L** | S/L/S/L/L/L/M/**S**/**M**/**L** | L/S/L/L/L/L/L/**L**/**L**/**L** |
| *P* | L/L/L/L/L/L/L/**L**/**S**/**L** | L/L/L/L/L/L/L/**S**/**L**/**L** | L/L/L/L/L/L/S/**L**/**L**/**L** |

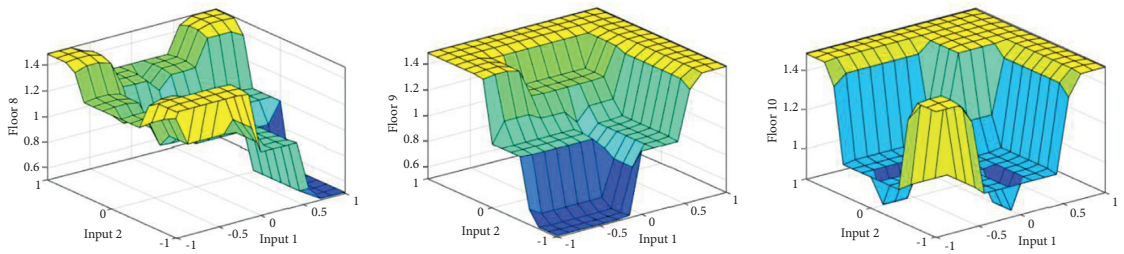


Figure 6: Curve surfaces of fuzzy rules for the top three floors: (a) rule surface for floor 8, (b) rule surface for floor 9, and (c) rule surface for floor 10.

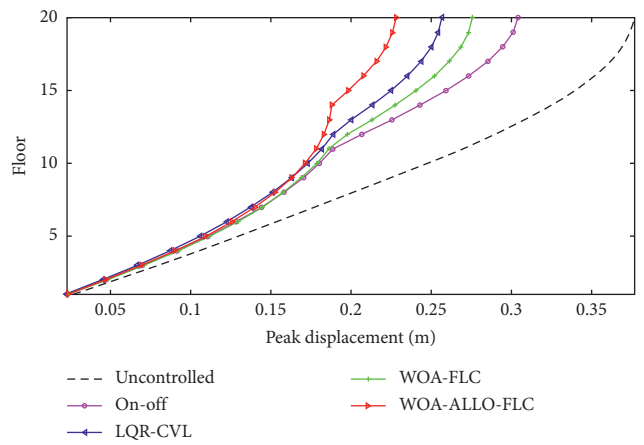


Figure 7: Comparison of the peak displacements of Building 1 among different control methods.

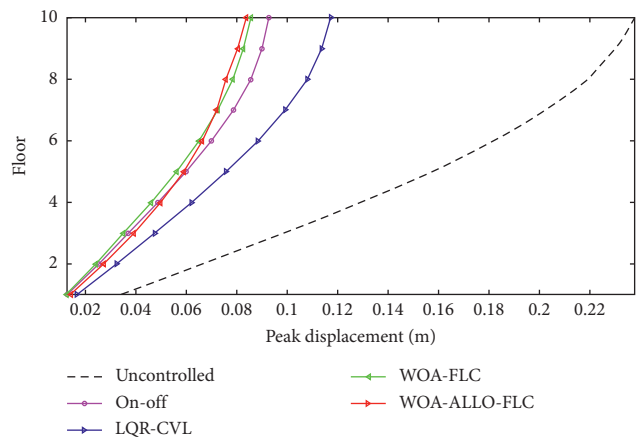


Figure 8: Comparison of the peak displacements of Building 2 among different control methods.

Table 8: Maximum responses (reduction ratios) with different control strategies.

| Maximum displacement | Building 1 | Building 2 |
|---|---|---|
| Uncontrolled | 0.3769 | 0.2378 |
| On-off | 0.3042 (19%) | 0.0927 (61%) |
| LQR-CVL | 0.2567 (32%) | 0.1172 (51%) |
| WOA-FLC | 0.2756 (27%) | 0.0855 (64%) |
| WOA-ALLO-FLC | 0.2281 (39%) | 0.0837 (65%) |

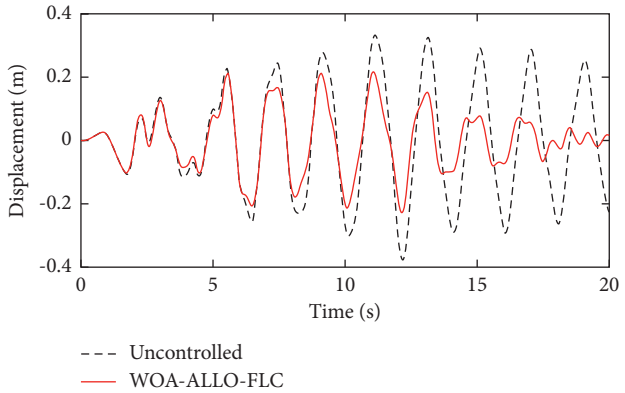


Figure 9: The top floor displacement response of Building 1.

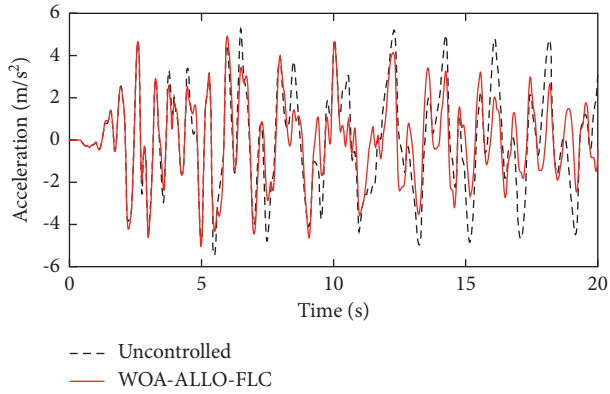


Figure 10: The top floor acceleration responses of Building 1.

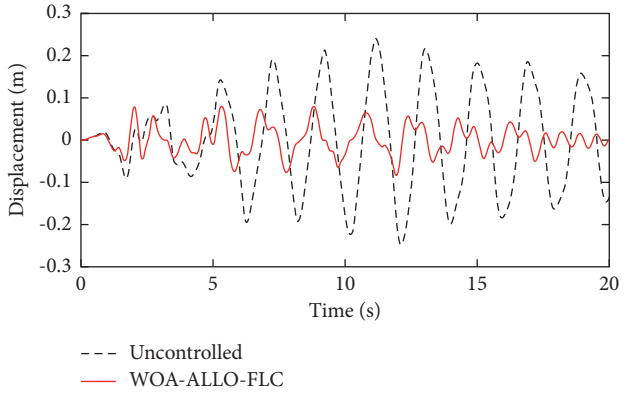


Figure 11: The top floor displacement responses of Building 2.

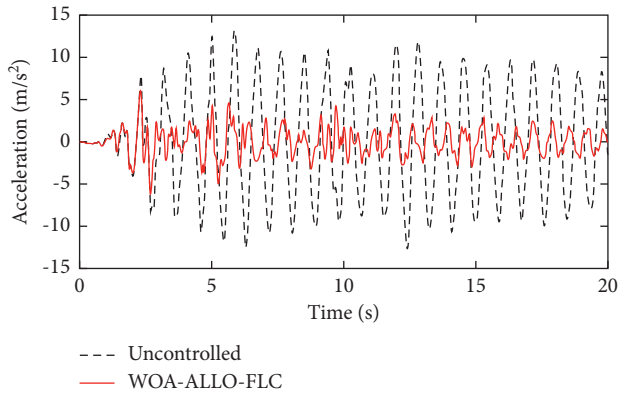


Figure 12: The top floor acceleration responses of Building 2.

Table 9: Comparison of the performance criteria among different control methods.

| Control strategy | On-off | LQR-CVL | WOA-FLC | WOA-ALLO-FLC |
|---|---|---|---|---|
| $J_{1,1}$ | 0.8071 | 0.6809 | 0.7313 | **0.6051** |
| $J_{1,2}$ | 0.3897 | 0.4927 | 0.3594 | **0.3518** |
| $J_{2,1}$ | 1.1096 | **0.8322** | 0.8696 | 0.9072 |
| $J_{2,2}$ | 0.5764 | 0.5938 | 0.5449 | **0.4680** |
| $J_{3,1}$ | 0.8742 | **0.8415** | 0.9000 | 0.8699 |
| $J_{3,2}$ | 0.3877 | 0.4919 | **0.3732** | 0.4192 |
| $J_{4,1}$ | 0.6984 | 0.6331 | 0.6727 | **0.5687** |
| $J_{4,2}$ | 0.2742 | 0.3036 | **0.2426** | 0.2755 |
| $J_{5,1}$ | 0.9058 | **0.7467** | 0.8051 | 0.8188 |
| $J_{5,2}$ | 1.2406 | 1.1399 | 1.0012 | **0.9664** |
| $J_{6,1}$ | 0.7278 | 0.6391 | 0.6782 | **0.5909** |
| $J_{6,2}$ | 0.2710 | 0.2972 | **0.2353** | 0.2516 |
| $J_7$ | 20 | 20 | 20 | **12** |

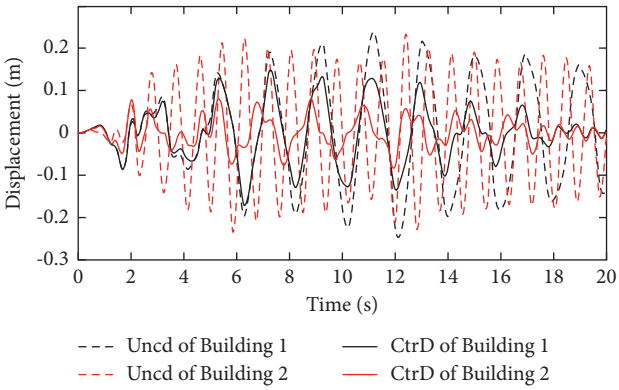


Figure 13: The displacement responses of the 10th floors with the WOA-ALLO-FLC and without control.

Table 10: Comparison of minimum anticollision gaps among different control methods.

| | Uncontrolled | On-off | LQR-CVL | WOA-FLC | WOA-ALLO-FLC |
|---|---|---|---|---|---|
| Minimum gap (m) | 0.3911 | 0.1970 (50%) | 0.1698 (57%) | 0.1627 (58%) | 0.1332 (66%) |

Time histories of the maximum (top floor) displacements and accelerations with the WOA-ALLO-FLC and without control for Building 1 are shown in Figures 9 and 10, respectively. Time histories of the corresponding responses for Building 2 are shown in Figures 11 and 12, respectively. The results show that the WOA-ALLO-FLC method can also simultaneously reduce the maximum accelerations of both buildings, especially for Building 2.

Apart from $J_{1,1}$ and $J_{1,2}$ defined in equation (27), a set of criteria is used to evaluate the performance of different control methods as follows:

$$J_{2,1}, J_{2,2} = \frac{\max\left|\ddot{x}^{c}(t)\right|}{\left|\ddot{x}_{\max}^{unc}\right|}, \quad J_{3,1}, J_{3,2} = \frac{\max\left|\mathrm{d}^{c}(t)\right|}{\left|\mathrm{d}_{\max}^{unc}\right|}, \tag{28}$$

$$J_{4,1}, J_{4,2} = \frac{\mathrm{rms}\left(x^{c}(t)\right)}{\mathrm{rms}\left(x_{top}^{unc}(t)\right)}, \quad J_{5,1}, J_{5,2} = \frac{\mathrm{rms}\left(\ddot{x}^{c}(t)\right)}{\mathrm{rms}\left(\ddot{x}_{top}^{unc}(t)\right)}, \tag{29}$$

$$J_{6,1}, J_{6,2} = \frac{\mathrm{rms}\left(\mathrm{d}^{c}(t)\right)}{\mathrm{rms}\left(\mathrm{d}_{top}^{unc}\right)}, \tag{30}$$

$$J7 = \text{total number of MR dampers},$$

where subscripts 1 and 2 refer to Buildings 1 and 2, respectively. $\ddot{x}_{\max}^{unc}$ and $d_{\max}^{unc}$ are the maximum acceleration and maximum interstory drift, respectively, of each uncontrolled building. $\ddot{x}^{c}(t)$ and $d^{c}(t)$ are the maximum acceleration and maximum interstory drift, respectively, of the corresponding floors of each controlled building. $x_{top}^{unc}(t)$, $\ddot{x}_{top}^{unc}(t)$, and $d_{top}^{unc}(t)$ are the displacement, acceleration, and interstory drift, respectively, of the top floor of each uncontrolled building. rms is the abbreviation of the root mean square. These performance indexes are compared in Table 9 where the numbers in bold font are the best index values. Among these 13 performance indexes, there are 7, 3, and 3 best quantities that are achieved by the WOA-ALLO-FLC, WOA-FLC, and on-off control methods, respectively. In addition, it is only the WOA-ALLO-FLC method that can obtain all the "smaller than 1" performance indexes, indicating that the proposed method can reduce all the displacement, acceleration, and interstory drift responses in terms of the maximum value and root mean square value, although the optimization objective for the design of WOA-ALLO-FLC is only to minimize the maximum displacements. It can be concluded that compared with the other three control methods, the proposed WOA-ALLO-FLC method performs best in reducing structural responses.

As observed from Figures 7 and 8, for both buildings, the higher the floors are, the larger the peak displacements will become. Therefore, a high risk of pounding is expected on the 10th floor of the adjacent buildings. The pounding reduction is examined by the investigation of the minimum separation gap required to avoid mutual impact (called anticollision gap in short) in view of the 10th-floor displacements of both buildings [36]. The 10th-floor displacements of both buildings with the WOA-ALLO-FLC and without control are shown in Figure 13, where UncD and CtrD represent the displacement without control and with WOA-ALLO-FLC, respectively. The figure demonstrates that the relative motion between the adjacent buildings is obviously abated by the proposed control method. The minimum anticollision spacing with different control strategies is compared in Table 10, where the reduction ratios of the controlled gaps and the uncontrolled gap are listed in the parentheses. The results indicate that the largest reduction ratio of 66% is achieved with the proposed strategy, meaning that this strategy is the most effective in pounding mitigation. The control effect of the LQR-CVL method is close to that of the WOA-FLC method, both of which outperform the on-off control method.

## 6. Conclusion

In this study, MR dampers are used as connection devices for adjacent structures, and an optimal design strategy for allocation and fuzzy control of MR dampers by use of WOA is proposed to enhance the seismic performance of adjacent structures. The main conclusions are listed as follows:

(1) WOA is very effective in designing the control strategy to minimize the maximum displacements of the adjacent buildings. The comparison results show that WOA is very promising as it outperforms GA, PSO, and CSA in terms of convergence accuracy. In addition, the robustness of WOA is close to that of CSA and better than that of GA and PSO.

(2) In other compared control methods, including on-off, LQR-CVL, and WOA-FLC (no allocation optimization is considered) methods, 20 MR dampers are used to connect the adjacent buildings, while in the proposed WOA-ALLO-FLC method, the adjacent buildings are connected using only 12 MR dampers. The results demonstrate that the proposed method with much less MR dampers shows comprehensive performance superiority over the other three control strategies in terms of the structural responses and pounding mitigation, which indicates that the optimal allocation of MR dampers is very necessary.

(3) Among all these compared control methods, it is only WOA-ALLO-FLC that can mitigate simultaneously all the displacement, acceleration, and interstory drift responses for the adjacent buildings. What is more, it can achieve the largest reduction ratios of 39% and 65% for the maximum displacements for Buildings 1 and 2, respectively, and obtain the largest reduction ratio of 66% for anticollision gap.

The proposed control strategy will enlighten investigation on the control system of novel high-rise structures as well as the adjacent structures with consideration of the factors such as nonlinear structural characteristics and pile-soil-structure interaction. Besides, the proposed optimization strategy can be further studied in terms of multi-objective optimization with the Pareto front solution.

## Nomenclature/Abbreviations

MR: Magnetorheological
MA: Metaheuristic algorithm

WOA: Whale optimization algorithm
PSO: Particle swarm optimization
GA: Genetic algorithm
CSA: Crow search algorithm
LQR: Linear quadratic regulator
CVL: Clipped voltage law
MF: Membership function
FLC: Fuzzy logic controller
ALLO: Allocation
$n$: Number of the floors of the shorter building
$n_i$: Number of the inputs of FLC
$N_{\text{para}}$: Total number of the parameters to be optimized
$n_o$: Number of the outputs of FLC
$n_{\text{imf}}$: Number of the MFs for each input
$n_{\text{omf}}$: Number of the MFs for each output
$n_{\text{rule}}$: Number of the fuzzy rules
$n_{\max D}$: Allowed maximum number of MR dampers linking the adjacent floors of the same height
$N_{\max D}$: Allowed maximum total number of MR dampers
rms: Root mean square.

## Data Availability

The data generated or analyzed during this study are included within the article.

## Conflicts of Interest

The authors declare that there are no conflicts of interest regarding the publication of this paper.

## Acknowledgments

This work was supported by the Scientific Research Foundation for the Introduction of Talents of Minjiang University, Fujian Province, under Grant no. MJY20029 and the Science and Technology Project Founded by Ningde City, Fujian Province, under Grant no. 20190006.

## References

[1] V. V. Bertero, "Observation of structural pounding," in *Proceedings of the International Conference on the Mexico Earthquake*, pp. 264–278, ASCE, New York, USA, September 1987.

[2] K. Kasai, V. Jeng, P. Patel, J. Munshi, and B. Maison, "Seismic pounding effects-survey and analysis," in *Proceedings of the 10th World Conference on Earthquake Engineering*, pp. 19–24, Madrid, Spain, July 1992.

[3] G. L. Cole, R. P. Dhakal, and F. M. Turner, "Building pounding damage observed in the 2011 Christchurch earthquake," *Earthquake Engineering & Structural Dynamics*, vol. 41, no. 5, pp. 893–913, 2012.

[4] S. Tesfamariam and M. Saatcioglu, "Seismic vulnerability assessment of reinforced concrete buildings using hierarchical fuzzy rule base modeling," *Earthquake Spectra*, vol. 26, no. 1, pp. 235–256, 2010.

[5] M. N. S. Hadi and M. E. Uz, "Investigating the optimal passive and active vibration controls of adjacent buildings based on performance indices using genetic algorithms," *Engineering Optimization*, vol. 47, no. 2, pp. 265–286, 2015.

[6] L. Zou, K. Huang, L. Wang, J. Butterworth, and X. Ma, "Vibration control of adjacent buildings considering pile-soil-structure interaction," *Journal of Vibration and Control*, vol. 18, no. 5, pp. 684–695, 2011.

[7] O. A. S. Al-Fahdawi, L. R. Barroso, and R. W. Soares, "Simple adaptive control method for mitigating the seismic responses of coupled adjacent buildings considering parameter variations," *Engineering Structures*, vol. 186, pp. 369–381, 2019.

[8] J.-S. Oh, K. Jeon, G.-W. Kim, and S.-B. Choi, "Dynamic analysis of semi-active MR suspension system considering response time and damping force curve," *Journal of Intelligent Material Systems and Structures*, vol. 32, no. 13, pp. 1462–1472, 2021.

[9] D. Q. Bui, N. Hung, and V. L. Hoang, "A new self-adaptive magneto-rheological damper for washing machines," *Smart Materials and Structures*, vol. 30, no. 3, pp. 1–12, 2021.

[10] S. Zhang, W. Shi, and Z. Chen, "Modeling and Parameter Identification of MR Damper Considering Excitation Characteristics and Current," *Shock And Vibration*, vol. 2021, pp. 1–17, Article ID 6691650, 2021.

[11] J. Katebi and S. M. Zadeh, "Time delay study for semi-active control of coupled adjacent structures using MR damper," *Structural Engineering & Mechanics*, vol. 58, no. 6, pp. 1127–1143, 2016.

[12] X. F. Lin, S. M. Chen, and W. Q. Lin, "Modified crow search algorithm based-fuzzy control of adjacent buildings connected by MR dampers considering soil-structure interaction," *Journal of Vibration and Control*, vol. 27, no. 1-2, pp. 57–72, 2021.

[13] G. Leitmann, "Semiactive control for vibration attenuation," *Journal of Intelligent Material Systems and Structures*, vol. 5, no. 6, pp. 841–846, 1994.

[14] S. J. Dyke, B. F. Spencer, M. K. Sain, and J. D. Carlson, "Modeling and control of magnetorheological dampers for seismic response reduction," *Smart Materials and Structures*, vol. 5, no. 5, pp. 565–575, 1996.

[15] S. K. Huang and C. H. Loh, "Combination of decentralized sliding mode control and online wavelet analysis for control of equipment with isolation system," *Structural Control and Health Monitoring*, vol. 26, no. 5, pp. 1–19, 2019.

[16] J. Wu, H. Zhou, Z. Liu, and M. Gu, "A load-dependent PWA-H∞ controller for semi-active suspensions to exploit the performance of MR dampers," *Mechanical Systems and Signal Processing*, vol. 127, pp. 441–462, 2019.

[17] S. M. A. Hashemi, H. Haji Kazemi, and A. Karamodin, "Localized genetically optimized wavelet neural network for semi-active control of buildings subjected to earthquake," *Structural Control and Health Monitoring*, vol. 23, no. 8, pp. 1074–1087, 2016.

[18] X. Tang, H. Du, S. Sun, D. Ning, Z. Xing, and W. Li, "Takagi-Sugeno fuzzy control for semi-active vehicle suspension with a magnetorheological damper and experimental validation," *IEEE*, vol. 22, no. 1, pp. 291–300, 2017.

[19] M. Abdeddaim, A. Ounis, and T. K. Datta, M. K. Shrimali, Retrofitting of a weaker building by coupling it to an adjacent stronger building using MR dampers," *Structural Engineering & Mechanics*, vol. 62, no. 2, pp. 197–208, 2017.

[20] M. J. Mahmoodabadi, M. B. S. Mottaghi, and A. Mahmodinejad, "Optimum design of fuzzy controllers for nonlinear systems using multi-objective particle swarm optimization," *Journal of Vibration and Control*, vol. 22, no. 3, pp. 769–783, 2016.

[21] S.-Y. Ok, J. Song, and K.-S. Park, "Optimal design of hysteretic dampers connecting adjacent structures using multi-objective

genetic algorithm and stochastic linearization method," *Engineering Structures*, vol. 30, no. 5, pp. 1240–1249, 2008.

[22] M. E. Uz and M. N. S. Hadi, "Optimal design of semi active control for adjacent buildings connected by MR damper based on integrated fuzzy logic and multi-objective genetic algorithm," *Engineering Structures*, vol. 69, no. 9, pp. 135–148, 2014.

[23] S. Mirjalili and A. Lewis, "The whale optimization algorithm," *Advances in Engineering Software*, vol. 95, pp. 51–67, 2016.

[24] Q.-V. Pham, S. Mirjalili, N. Kumar, M. Alazab, and W.-J. Hwang, "Whale optimization algorithm with applications to resource allocation in wireless networks," *IEEE Transactions on Vehicular Technology*, vol. 69, no. 4, pp. 4285–4297, 2020.

[25] H. Ebrahimgol, M. Aghaie, A. Zolfaghari, and A. Naserbegi, "A novel approach in exergy optimization of a WWER1000 nuclear power plant using whale optimization algorithm," *Annals of Nuclear Energy*, vol. 145, Article ID 107540, 2020.

[26] S. Sharmila and S. Vijayarani, "Association rule mining using fuzzy logic and whale optimization algorithm," *Soft Computing*, vol. 25, no. 1, pp. 1431–1446, 2021.

[27] Z. Yan, J. Zhang, and J. Tang, "Modified whale optimization algorithm for underwater image matching in a UUV vision system," *Multimedia Tools and Applications*, vol. 80, no. 11, pp. 187–213, 2021.

[28] M. Huang, X. Cheng, and Y. Lei, "Structural damage identification based on substructure method and improved whale optimization algorithm," *Journal of Civil Structural Health Monitoring*, vol. 11, no. 2, pp. 351–380, 2021.

[29] M. M. Draz and S. Abdulkader, M. G. Gafar, Code smell detection using whale optimization algorithm," *Computers, Materials & Continua*, vol. 68, no. 2, pp. 1919–1935, 2021.

[30] B. F. Spencer, S. J. Dyke, M. K. Sain, and J. D. Carlson, "Phenomenological model for magnetorheological dampers," *Journal of Engineering Mechanics*, vol. 123, no. 3, pp. 230–238, 1997.

[31] M. E. Uz and P. Sharafi, "Investigation of the optimal semi-active control strategies of adjacent buildings connected with magnetorheological dampers," *International Journal of Optimization in Civil Engineering*, vol. 6, no. 4, pp. 523–547, 2016.

[32] G. Yan and L. L. Zhou, "Integrated fuzzy logic and genetic algorithms for multi-objective control of structures using MR dampers," *Journal of Sound and Vibration*, vol. 296, no. 1, pp. 368–382, 2006.

[33] X. Lin, S. Chen, and G. Huang, "A shuffled frog-leaping algorithm based mixed-sensitivity H∞ control of a seismically excited structural building using MR dampers," *Journal of Vibration and Control*, vol. 24, no. 13, pp. 2832–2852, 2018.

[34] M. Bozorgvar and S. M. Zahrai, "Semi-active seismic control of a 9-story benchmark building using adaptive neural-fuzzy inference system and fuzzy cooperative coevolution," *Smart Materials and Structures*, vol. 23, no. 1, pp. 1–14, 2019.

[35] A. Askarzadeh, "A novel metaheuristic method for solving constrained engineering optimization problems: crow search algorithm," *Computers & Structures*, vol. 169, pp. 1–12, 2016.

[36] M. Abdeddaim, A. Ounis, N. Djedoui, and M. K. Shrimali, "Pounding hazard mitigation between adjacent planar buildings using coupling strategy," *Journal of Civil Structural Health Monitoring*, vol. 6, no. 3, pp. 603–617, 2016.